

Tail Risk Management with Puts and Trend Following: A CVaR Framework for Crashes and Drawdowns

Miquel Noguer i Alonso

Artificial Intelligence Finance Institute (AIFI)

Ali Al-Fallouji

Mirabaud Group

July 1, 2026

Abstract

Tail-risk management is not only an instrument-selection problem. It is an allocation problem across loss mechanisms: abrupt crash states, volatility repricing, and persistent drawdowns require different forms of protection. This paper develops a continuous-time CVaR framework that places two common protection sleeves—long out-of-the-money put options and systematic trend-following overlays—inside one coherent tail-risk mandate. The option sleeve is modeled as a marked-to-market traded asset, so premium drag, diffusion exposure, and jump repricing enter through its physical return process rather than through inconsistent terminal-payoff accounting. The resulting Markov state contains wealth, spot, stochastic variance, and an exponentially weighted log-return signal, and we derive the associated Hamilton–Jacobi–Bellman equation in viscosity form. The main analytical separation is temporal: convex insurance reprices immediately on jump impact, whereas trend following is late on the first shock because its signal must cross zero, but becomes increasingly defensive during persistent drawdowns without requiring fresh option premium. We then give sufficient and local conditions for an interior hybrid allocation, derive a CVaR policy-gradient identity, and introduce a four-axis diagnostic layer separating conditional convexity, tail-event reliability, non-stress carry, and drawdown persistence. Stylized Monte Carlo experiments illustrate the mechanism: fixed equal-weight hybrids and grid-optimized hybrids reduce terminal CVaR relative to either pure sleeve in the reported regimes, while the exact weight location remains calibration-dependent. The contribution is a transparent risk-management framework for deciding how much convex crash protection and how much signal-driven drawdown protection a mandate should hold.

Keywords: tail-risk management; tail-risk hedging; put options; trend following; conditional value-at-risk; stochastic control; Hamilton–Jacobi–Bellman equation; jump diffusion; stochastic volatility; policy gradient; hedge-quality diagnostics.

1 Introduction

Institutions that care about large drawdowns do not face a generic portfolio problem. They face a state-contingent downside problem: losses arrive through a mixture of abrupt jumps, volatility spikes, and persistent directional selloffs. That is exactly where classical mean-variance analysis is weakest. It treats upside and downside dispersion symmetrically and gives no special role to the shape of the left tail (Markowitz, 1952).

We therefore use the phrase *tail-risk management* deliberately. A hedge is an instrument-level object; a tail-risk mandate is a portfolio-level design problem. The mandate must decide how much convexity, reliability, carry drag, and persistence it is willing to hold in order to reduce expected loss in the left tail. Put options and trend following are two sleeves inside that broader allocation problem, not mutually exclusive answers to the same question.

In practice, two very different hedging technologies dominate that left-tail problem. The first is explicit convex insurance through long out-of-the-money index puts. Their appeal is obvious: if the market gaps down, the option reprices immediately and contractually. The second is dynamic trend-following, implemented through signal-driven futures or overlay trades that progressively cut or reverse exposure as price action deteriorates. Trend is slower, but it can be positively carried over long samples and performs especially well when losses unfold over time rather than on impact (Hurst et al., 2017; Ilmanen et al., 2020).

Those facts suggest a simple economic principle: the best hedge depends on the transmission mechanism of the drawdown. Puts are strongest against sudden crash states, but systematic option rolling often carries a persistent premium drag because index implied variance tends to exceed subsequently realized variance (Broadie et al., 2009; Israelov and Nielsen, 2017). Trend has the opposite profile. It is not contractual and can be caught long during violent reversals, yet it often works well in prolonged selloffs because it converts persistent negative returns into progressively more defensive positioning (Moskowitz et al., 2012; Hurst et al., 2017).

The systematic hedging literature also suggests that hedge quality is not a one-dimensional object. It is often decomposed into conditional convexity or asymmetric co-movement with the market in bad states, reliability or the probability of producing a positive payoff in tail events, carry outside stress, and persistence across drawdown horizons. Downside-risk models emphasize that market exposures can change precisely when the price of risk is high (Lettau et al., 2014); asset-pricing theory puts the cost of carry at the center of expected-return trade-offs (Cochrane, 2005); and the managed-futures and time-series-momentum evidence highlights the importance of drawdown duration (Moskowitz et al., 2012; Hurst et al., 2013; Hurst et al., 2017). A scalar CVaR criterion aggregates these mechanisms. That aggregation is useful for optimization, but it can hide which economic channel is actually providing protection.

What is still missing is a single framework that puts both channels inside the same tail-risk objective with internally consistent accounting while also making these hedge-quality dimensions explicit. This paper provides that framework. We model the risky asset with Heston-type stochastic variance and negative jumps, let the investor choose both directional exposure and convex-overlay exposure, and evaluate the resulting strategy

through terminal-loss CVaR using the Rockafellar–Uryasev representation (Rockafellar and Uryasev, 2000; Acerbi, 2002; Artzner et al., 1999). The resulting control problem produces five concrete improvements over existing heuristic discussions.

Contributions. The paper makes five contributions.

1. It formulates convex insurance and dynamic trend inside one continuous-time CVaR-minimization problem with a fully Markov state. Crucially, the option overlay is handled as a traded mark-to-market asset, which resolves the premium-accounting inconsistency that often appears in terminal-payoff comparisons.
2. It makes explicit a four-axis hedge-quality diagnostic—conditional convexity, tail-event reliability, non-stress carry, and drawdown persistence—and shows how these dimensions can enter the problem either as constraints or as penalty terms around the CVaR objective.
3. It derives the jump-diffusion HJB equation in viscosity form for the augmented state consisting of wealth, spot, variance, and the trend signal.
4. It gives analytical comparative statics that separate the two hedge channels: puts hedge jump states on impact, whereas trend hedges drawdowns that last long enough for the signal to cross through zero and turn the portfolio defensive.
5. It derives a CVaR policy-gradient identity and connects it to a fast simulation pipeline used in our numerical experiments, which delivers stylized but informative regime evidence.

Scope. This is a theory-first paper with stylized Monte Carlo evidence. It is not a full historical backtest, and it does not claim a complete option-surface calibration. In particular, the experiments use a fast Black–Scholes proxy for option valuation inside the simulation section. That choice is appropriate for illustrating the economics of the hybrid hedge, but it should not be confused with a production empirical implementation.

The empirical claims are therefore stated in the language of *mechanism validation*: the simulations check whether the model reproduces the expected ranking of protection channels across crash, prolonged-bear, and volatility states. They do not establish universal dominance of the hybrid over every possible option program or trend specification. The reported hybrid optima are best read as calibrated examples of the allocation logic developed below.

The four-axis diagnostic layer should be read in the same spirit. It is not yet a full historical taxonomy of all tradable hedges. It is a transparent way to label the mechanisms that the CVaR objective otherwise compresses into a single number, and it provides a bridge from the two-channel theoretical model to a larger structuring universe.

The analysis draws on continuous-time portfolio choice (Merton, 1969; Merton, 1971), stochastic control for jump diffusions (Øksendal and Sulem, 2005; Fleming and Soner, 2006; Pham, 2009), the economics of option-based crash protection (Bhansali, 2014; Broadie et al., 2009; Israelov and Nielsen, 2017), and the empirical literature on trend-following

and time-series momentum (Moskowitz et al., 2012; Hurst et al., 2013; Hurst et al., 2017; Ilmanen et al., 2020). The rest of the paper is organized as follows. Section 2 introduces the market environment and the two hedge channels. Section 3 states the CVaR objective. Section 4 gives the dynamic control problem and its HJB characterization. Section 5 contains the key comparative statics and a reduced-form interior-hybrid result. Section 6 derives the policy-gradient identity. Section 7 reports stylized Monte Carlo evidence from our numerical experiments. Section 8 and Section 9 close.

2 Economic setup

2.1 Asset dynamics

Let $(\Omega, \mathcal{F}, \{\mathcal{F}_t\}_{t \in [0, T]}, \mathbb{P})$ be a filtered probability space satisfying the usual conditions. The risky asset price S_t follows a stochastic-volatility jump diffusion,

$$\frac{dS_t}{S_{t-}} = \mu dt + \sqrt{v_t} dW_t^S + (e^\zeta - 1) dN_t, \quad (1)$$

where N_t is a Poisson process with intensity $\lambda > 0$ and i.i.d. log-jump sizes ζ with distribution F_ζ supported on a bounded interval

$$\zeta \in [\underline{\zeta}, \bar{\zeta}] \subset \mathbb{R}, \quad \underline{\zeta} < 0 < \bar{\zeta}. \quad (2)$$

Boundedness of the jump support is used below to guarantee strict wealth positivity under two-sided directional exposure. In practice F_ζ can be taken as a truncated Gaussian $\mathcal{N}(\mu_\zeta, \sigma_\zeta^2)$ restricted to $[\underline{\zeta}, \bar{\zeta}]$; the truncation bounds are non-binding in the stylized calibration of Table 2 because $\bar{\zeta}$ is set at several standard deviations above μ_ζ . The variance process is of Heston type (Heston, 1993):

$$dv_t = \kappa(\theta - v_t)dt + \xi\sqrt{v_t}dZ_t, \quad dW_t^S dZ_t = \rho dt, \quad (3)$$

with $\kappa, \theta, \xi > 0$ and $\rho \in (-1, 0)$. The negative correlation captures the leverage effect. Throughout we assume the Feller condition $2\kappa\theta > \xi^2$ holds, which keeps v_t strictly positive almost surely and simplifies the boundary analysis of the integro-PDE below.

For signal construction it is convenient to work with log-prices. Writing $y_t := \log S_t$, Itô's formula for jump diffusions yields

$$dy_t = \left(\mu - \frac{1}{2}v_t\right)dt + \sqrt{v_t}dW_t^S + \zeta dN_t. \quad (4)$$

Assumption 2.1 (Admissible controls). The investor chooses a progressively measurable pair $c_t = (\pi_t, q_t)$ taking values in the compact set $\mathcal{K} = [\underline{\pi}, \bar{\pi}] \times [0, \bar{q}]$, where π_t is the directional exposure to the risky asset and q_t is the return exposure to the convex overlay. Directional exposure is two-sided: $\underline{\pi} < 0 \leq \bar{\pi}$. To guarantee strict wealth positivity across both directions of jump, the directional bounds and the jump support in (2) are required

to satisfy the two-sided leverage conditions

$$\bar{\pi} + \bar{q} < 1, \quad 1 + \underline{\pi}(e^{\bar{\zeta}} - 1) - \bar{q} > 0, \quad (5)$$

together with the overlay bound $R_P \geq -1$ used in Lemma 4.1 below. The first condition controls the worst-case *downside* jump for a long position (where $e^{\bar{\zeta}} - 1 \geq -1$ and $R_P \geq -1$); the second controls the worst-case *upside* jump for a short position. Controls satisfy $\mathbb{E}[\int_0^T (\pi_t^2 + q_t^2) dt] < \infty$.

A risk-free asset is available, but we work in excess-return units and set the short rate to zero throughout.

2.2 Convex insurance as a traded overlay

We need to distinguish two economic objects that are often conflated in the structured-hedging literature but which have different mathematical structure: a *fixed-maturity* traded option, and a *rolled* constant-maturity trading strategy. The continuous-time theory below works with the former; the Monte Carlo experiments in Section 7 implement the latter. The two are related through a simple roll-date correction that we make explicit at the end of this subsection.

The fixed-maturity overlay. Let $T_{\text{opt}} \in (0, T]$ be a fixed option maturity and let $P(t, s, v)$ denote the marked-to-market price, at time $t < T_{\text{opt}}$ and state $(S_t, v_t) = (s, v)$, of a European option with payoff $\Phi(S_{T_{\text{opt}}})$ at maturity. In the put case of interest, $\Phi(S) = (K - S)^+$ with $K \in (0, \infty)$. The overlay is a genuine traded asset between inception and maturity, and the investor can hold fractional positions of notional return exposure q_t to its physical return process.

Assumption 2.2 (Overlay regularity). There exists a measure \mathbb{Q} , equivalent to \mathbb{P} on \mathcal{F}_T , under which $P(t, S_t, v_t)$ is the discounted martingale price of the option payoff $\Phi(S_{T_{\text{opt}}})$. The map $P : [0, T_{\text{opt}}] \times (0, \infty)^2 \rightarrow (0, \infty)$ is once continuously differentiable in time and twice continuously differentiable in (s, v) on $[0, T_{\text{opt}}] \times (0, \infty)^2$, with locally bounded derivatives, and $P(t, s, v) \geq (K - s)^+ \geq 0$. The overlay's physical return process is obtained by applying Itô's formula to $P(t, S_t, v_t)$ under \mathbb{P} .

Define the option elasticity and vega loading by

$$\delta_P(t, s, v) := \frac{s P_s(t, s, v)}{P(t, s, v)}, \quad \nu_P(t, s, v) := \frac{P_v(t, s, v)}{P(t, s, v)}. \quad (6)$$

Under Assumption 2.2, the overlay return can be written as

$$\frac{dP_t}{P_{t^-}} = \mu_P(t, S_t, v_t) dt + \delta_P(t, S_t, v_t) \sqrt{v_t} dW_t^S + \nu_P(t, S_t, v_t) \xi \sqrt{v_t} dZ_t + R_P(t, S_{t^-}, v_t; \zeta) dN_t, \quad (7)$$

where

$$R_P(t, s, v; \zeta) := \frac{P(t, se^{\zeta}, v) - P(t, s, v)}{P(t, s, v)}. \quad (8)$$

The physical drift collects the remaining terms from Itô's formula:

$$\mu_P(t, s, v) := \frac{1}{P} \left(P_t + \mu s P_s + \kappa(\theta - v) P_v + \frac{1}{2} v s^2 P_{ss} + \rho \xi v s P_{sv} + \frac{1}{2} \xi^2 v P_{vv} \right). \quad (9)$$

This convention writes the jump contribution in raw dN_t form. Thus μ_P is the continuous drift of the overlay between jump arrivals. The unconditional instantaneous physical drift of P is $\mu_P + \lambda \mathbb{E}_\zeta[R_P(t, s, v; \zeta)]$. Equivalently, one could rewrite (7) with the compensated process $d\tilde{N}_t = dN_t - \lambda dt$ and absorb the compensator into the drift. We keep the raw-jump convention because it makes crash-state repricing explicit in the wealth equation and in the HJB jump operator.

Proposition 2.3 (Marked-to-market option decomposition). *Under Assumption 2.2, the dynamics in (7) hold. The jump return is the immediate percentage repricing of the overlay when the underlying moves from s to se^ζ .*

Proof. Apply Itô's formula for jump diffusions to the semimartingale $P(t, S_t, v_t)$. The continuous part produces the drift and the two diffusive loadings. The jump part is exactly the mark-to-market repricing $P(t, S_{t-}e^\zeta, v_t) - P(t, S_{t-}, v_t)$ divided by the pre-jump price. \square

Remark 2.4 (Where carry enters). The option premium is not ignored anywhere in this formulation. It is encoded in P_t and therefore in the overlay's physical drift μ_P . Historical evidence suggests that this drift is often negative for systematically rolled index puts because of the variance risk premium (Broadie et al., 2009; Israelov and Nielsen, 2017). The continuous-time theory below needs only the physical return process in (7); it does not require the premium to be modeled separately at terminal time.

The rolled-strategy implementation. In the Monte Carlo experiments of Section 7 the overlay is implemented as a self-financing trading rule rather than a single fixed-maturity contract. At each roll date $\tau_k = k\Delta$, $k = 0, 1, \dots$, the investor simultaneously (i) liquidates the previous contract at its prevailing market price $P^{(k-1)}(\tau_k, S_{\tau_k}, v_{\tau_k})$ and (ii) enters a fresh one-month 10% OTM put with maturity $T_{\text{opt}}^{(k)} = \tau_k + \Delta_{\text{opt}}$. *The rolls occur strictly before the natural expiry of the incumbent contract:* concretely we take $\Delta < \Delta_{\text{opt}}$ so that at each roll τ_k the outgoing contract has residual time value $T_{\text{opt}}^{(k-1)} - \tau_k = \Delta_{\text{opt}} - \Delta > 0$. In the simulations, $\Delta = 21$ trading days and $\Delta_{\text{opt}} = 30$ calendar days, so the outgoing contract has roughly nine calendar days of residual time value at every roll. Because the overlay state is (S_t, v_t) with $v_t > 0$ and the residual time to expiry is bounded below by $\Delta_{\text{opt}} - \Delta > 0$, the incumbent price $P^{(k-1)}(\tau_k, S_{\tau_k}, v_{\tau_k})$ is strictly positive almost surely and the roll ratio below is bounded.

Let $P^{(k)}(t, s, v)$ denote the fixed-maturity price of the k -th contract between τ_k and τ_{k+1} . The rolled strategy wealth P_t^{roll} evolves as $P^{(k)}(t, S_t, v_t)$ on $(\tau_k, \tau_{k+1}]$, with a self-financing discontinuity at each τ_{k+1} that exchanges the still-live incumbent contract for a

fresh one at market. In continuous time,

$$\frac{dP_t^{\text{roll}}}{P_{t^-}^{\text{roll}}} = \frac{dP_t^{(k)}}{P_{t^-}^{(k)}} \mathbf{1}_{(\tau_k, \tau_{k+1})}(t) + \underbrace{\left(\frac{P^{(k+1)}(\tau_{k+1}, S_{\tau_{k+1}}, v_{\tau_{k+1}})}{P^{(k)}(\tau_{k+1}, S_{\tau_{k+1}}, v_{\tau_{k+1}})} - 1 \right)}_{=: \eta_{k+1}} d\mathbf{1}_{\{t \geq \tau_{k+1}\}}. \quad (10)$$

Between rolls, P^{roll} has exactly the dynamics (7) for a fixed-maturity contract. At each roll τ_{k+1} , the pre-expiry convention above guarantees $P^{(k)}(\tau_{k+1}, \cdot) > 0$, so η_{k+1} is a well-defined finite return. Economically, η_{k+1} captures the wealth-fraction change when the portfolio substitutes the incumbent contract for a fresh constant-maturity contract at prevailing market prices. All systematic rolling costs — transaction costs, bid–ask spread, and the variance-risk-premium drag cited in Remark 2.4 — are absorbed into η_{k+1} and into the between-roll drift μ_P . An equivalent implementation rebalances a fixed wealth fraction (or a fixed premium budget) into the new contract and charges the residual cash flow to the risk-free account; under bounded roll ratios the two implementations coincide at the level of portfolio returns, so we retain the notional form (10) for consistency with the wealth equation below. Assumption 2.2 applies to each $P^{(k)}$ individually. The theoretical HJB analysis below is stated for the fixed-maturity object $P(t, s, v)$; the rolled-strategy object P_t^{roll} inherits those dynamics with the additional scheduled but state-dependent jump term in (10). It can be used directly inside the CVaR problem without modification, provided the roll dates $\{\tau_k\}$ are fixed in advance and the roll ratios η_{k+1} are bounded (as they are under the pre-expiry convention). In the stylized simulations we measure $P(t, s, v)$ through a Black–Scholes proxy calibrated to rolling realized volatility; this is not consistent with the Heston–jump specification of (1)–(3), and the magnitudes of carry drag and crash-state repricing are inherited from this proxy, so the reported CVaR levels and hybrid-weight location should be read as illustrative rather than invariant to the pricing model. A full Heston–jump pricing of each $P^{(k)}$, as part of a follow-up empirical calibration to a live option surface, is a natural extension.

2.3 Trend signal and filtering bridge

Define the exponentially weighted moving-average signal on log-returns by

$$M_t := \int_0^t e^{-\gamma(t-u)} dy_u, \quad \gamma > 0. \quad (11)$$

Because dy_u is a log-return increment, M_t is dimensionless and can be fed directly into a position map f . The signal dynamics are

$$dM_t = dy_t - \gamma M_t dt, \quad (12)$$

so a log-jump of size ζ moves the signal by exactly the same amount: $\Delta M_t = \zeta$. This unit consistency is important. It means that the reversal condition for trend can be stated in the same scale as the jump itself.

Take the directional exposure to be of the form

$$\pi_t = f(M_t), \quad (13)$$

where f is increasing and odd, for example $f(m) = \tanh(\beta m)$.

A complementary interpretation comes from modelling log-returns directly as noisy observations of a latent trend. Fix a discretization step $\Delta > 0$ and let $r_k := y_{k\Delta} - y_{(k-1)\Delta}$ denote the log-return over the k -th interval. Consider the local-level state-space model

$$r_k = \mu_k + \varepsilon_k, \quad \varepsilon_k \sim \mathcal{N}(0, \sigma_\varepsilon^2), \quad (14)$$

$$\mu_k = \mu_{k-1} + \omega_k, \quad \omega_k \sim \mathcal{N}(0, \sigma_\omega^2), \quad (15)$$

in which μ_k is a latent drift rate and ε_k, ω_k are independent Gaussian noises. The steady-state Kalman filter reduces to an EWMA on returns with constant gain $\kappa^* \in (0, 1)$ determined by the signal-to-noise ratio $\sigma_\omega^2/\sigma_\varepsilon^2$: the one-step filtered estimate satisfies $\hat{\mu}_k = \kappa^* r_k + (1 - \kappa^*) \hat{\mu}_{k-1}$. Summing from the origin shows that $\hat{\mu}_k$ is an exponentially weighted moving average of past returns, which is the continuous-time limit of (11) up to scaling. This provides a clean bridge between signal extraction and the control problem: trend is a filtered estimate of persistent directional motion in returns rather than an ad hoc trading rule, and the signal is defined on the same scale (log-returns) on which the control action operates.

Lemma 2.5 (Signal mechanics). *Assume f is odd and strictly increasing.*

(i) *If a log-jump $\zeta < 0$ occurs at time τ , then $M_\tau = M_{\tau-} + \zeta$. The position changes sign on impact if and only if*

$$\zeta < -M_{\tau-}. \quad (16)$$

(ii) *Suppose instead that after time τ the asset experiences a gradual deterministic draw-down with $dy_t = -c dt$ for $c > 0$ and no further jumps. If $M_\tau > 0$, then for $t \geq \tau$,*

$$M_t = -\frac{c}{\gamma} + \left(M_\tau + \frac{c}{\gamma}\right) e^{-\gamma(t-\tau)}. \quad (17)$$

The signal crosses zero at

$$t^* = \tau + \frac{1}{\gamma} \log\left(1 + \frac{\gamma M_\tau}{c}\right), \quad (18)$$

provided the drawdown lasts that long.

Proof. Part (i) is immediate from (12): a log-jump of size ζ enters both dy_t and M_t one-for-one. Because f is odd and strictly increasing, $f(M_{\tau-} + \zeta) < 0$ if and only if $M_{\tau-} + \zeta < 0$.

For part (ii), under $dy_t = -c dt$ and no jumps, (12) becomes the ODE $dM_t/dt = -c - \gamma M_t$. Solving it on $[\tau, \infty)$ gives (17). Setting $M_t = 0$ yields (18). \square

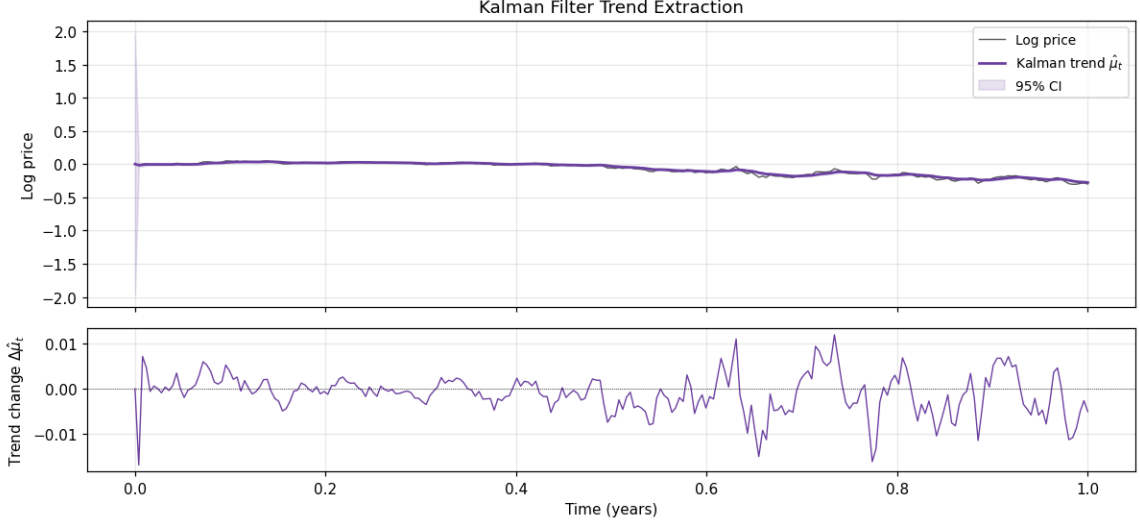


Figure 1: Kalman-filter trend extraction on a representative simulated path from our experiments. The top panel shows the log price together with the filtered latent trend and a 95% band. The bottom panel shows filtered trend increments. At steady state the Kalman recursion is an EWMA, which is the signal used in the control problem.

3 Tail-risk objective

We work throughout with the log-loss convention

$$L := -\log(X_T/X_0), \quad (19)$$

i.e. terminal loss is measured on the continuously compounded scale. This is equivalent to $L = -\log X_T$ when $X_0 = 1$ (which we assume without loss of generality), and matches the scale on which the stylized Monte Carlo CVaRs reported in Section 7 are computed. The log-loss convention is also convenient because post-jump wealth is strictly positive under Lemma 4.1, so $\log X_T$ is almost surely finite. For a confidence level $\alpha \in (0, 1)$, the Value-at-Risk and Conditional Value-at-Risk are

$$\text{VaR}_\alpha(L) := \inf\{\ell \in \mathbb{R} : \mathbb{P}(L \leq \ell) \geq \alpha\}, \quad (20)$$

and

$$\text{CVaR}_\alpha(L) := \mathbb{E}[L \mid L \geq \text{VaR}_\alpha(L)]. \quad (21)$$

The conditional-expectation form (21) requires the loss distribution to be continuous at the α -quantile. The Rockafellar–Uryasev representation below is valid without this restriction and is the formulation used throughout the paper. The representation of Rockafellar and Uryasev (2000) is central:

$$\text{CVaR}_\alpha(L) = \min_{\eta \in \mathbb{R}} \left\{ \eta + \frac{1}{1-\alpha} \mathbb{E}[(L - \eta)^+] \right\}. \quad (22)$$

It converts a tail expectation into a stochastic program with an auxiliary scalar η , which is exactly what makes dynamic programming feasible.

Remark 3.1 (Pre-commitment CVaR). Terminal CVaR is not in general a dynamically

time-consistent risk measure: an optimal policy for a terminal-CVaR problem at time $t = 0$ need not remain optimal for the corresponding tail problem at a later time $t \in (0, T)$ (Artzner et al., 1999; Rockafellar and Uryasev, 2000). The framework in this paper is therefore interpreted as a *pre-commitment* problem: at $t = 0$ the investor commits to a feedback policy (π_t, q_t) and an auxiliary threshold η by jointly minimizing the Rockafellar–Uryasev expression in (22); for any fixed η , the inner expectation is a standard terminal-cost expected-value problem and admits a dynamic programming representation, which we exploit in the HJB analysis below. This is consistent with almost all of the applied CVaR control literature. Fully time-consistent dynamic risk measures — such as recursive composition of one-period CVaR kernels — are a separate construction and are not the object of this paper.

3.1 Diagnostic decomposition of hedge quality

The CVaR objective is deliberately scalar: it ranks policies by the expected loss inside the left tail. For interpretation and structuring, however, it is useful to decompose the protection mechanism into observable hedge-quality dimensions. Fix a baseline market portfolio with terminal loss L^0 and define the stress set

$$\mathcal{A}_\alpha^0 := \{L^0 \geq \text{VaR}_\alpha(L^0)\}. \quad (23)$$

For a tradable hedge sleeve i with horizon return R_i and market return R_M , define the downside and normal-state betas

$$\beta_i^- := \frac{\text{Cov}(R_i, R_M \mid R_M \leq q_\alpha^M)}{\text{Var}(R_M \mid R_M \leq q_\alpha^M)}, \quad \beta_i^0 := \frac{\text{Cov}(R_i, R_M \mid R_M > q_\alpha^M)}{\text{Var}(R_M \mid R_M > q_\alpha^M)}, \quad (24)$$

where q_α^M is a lower-tail market-return quantile. A simple empirical conditional-convexity score is then

$$\text{Conv}_{i,\alpha} := -(\beta_i^- - \beta_i^0). \quad (25)$$

For a protective hedge, a high value means that market beta becomes more negative in bad states. This is an empirical co-movement proxy for conditional convexity; in the option component of the model, the structural source is the jump repricing $R_P(t, s, v; \zeta)$ and the curvature of P .

The other three dimensions can be measured on the same simulated or empirical paths:

$$\text{Hit}_{i,\alpha} := \mathbb{P}(R_i > 0 \mid \mathcal{A}_\alpha^0), \quad (26)$$

$$\text{Carry}_{i,\alpha} := -\mathbb{E}[R_i \mid (\mathcal{A}_\alpha^0)^c], \quad (27)$$

$$\text{Pers}_{i,h,d} := \mathbb{P}\left(\sum_{j=1}^h R_{i,t+j} > 0 \mid \mathcal{D}_{t,h,d}\right), \quad (28)$$

where $\mathcal{D}_{t,h,d}$ denotes a drawdown episode of duration h and depth at least d . Thus reliability is the tail-event hit ratio, carry is the non-stress drag of the sleeve, and persistence is the probability that the hedge continues to help over a multi-period

Table 1: Four hedge-quality dimensions and their role in the present model.

Dimension	Diagnostic object	Model counterpart
Conditional convexity	Downside co-movement asymmetry, measured for example by $\text{Conv}_{i,\alpha}$	Put jump repricing $R_P(t, s, v; \zeta)$, option elasticity δ_P , and curvature of P
Reliability	Tail hit ratio $\text{Hit}_{i,\alpha} = \mathbb{P}(R_i > 0 \mid \mathcal{A}_\alpha^0)$	Whether the sleeve pays in the same states that determine CVaR
Carry	Non-stress expected drag $\text{Carry}_{i,\alpha}$	Physical overlay drift μ_P and the premium drag of rolled convex insurance
Persistence	Multi-period drawdown protection $\text{Pers}_{i,h,d}$	Signal half-life γ^{-1} , reversal time $t^* - \tau$, and trend exposure $f(M_t)$

These diagnostics do not replace CVaR. They explain which mechanism reduces CVaR and provide economically interpretable constraints for implementation.

drawdown rather than only on the initial shock.

This decomposition leads to two implementable variants of the baseline problem. The first is a constrained version,

$$\begin{aligned}
 \min_{\theta} \quad & \text{CVaR}_\alpha(L(\theta)) \\
 \text{s.t.} \quad & \text{Conv}_{\theta,\alpha} \geq \underline{C}, \quad \text{Hit}_{\theta,\alpha} \geq \underline{H}, \\
 & \text{Carry}_{\theta,\alpha} \leq \overline{K}, \quad \text{Pers}_{\theta,h,d} \geq \underline{P},
 \end{aligned} \tag{29}$$

where θ parameterizes the hedge policy or sleeve weights. The second is a penalized multi-objective version,

$$\min_{\theta} \text{CVaR}_\alpha(L(\theta)) + \lambda_K \text{Carry}_{\theta,\alpha} + \lambda_F (1 - \text{Hit}_{\theta,\alpha}) + \lambda_D (1 - \text{Pers}_{\theta,h,d}) - \lambda_C \text{Conv}_{\theta,\alpha}. \tag{30}$$

The multipliers have a direct economic interpretation. A crash-sensitive mandate places high weight on conditional convexity and hit ratio; a cost-sensitive mandate puts more weight on carry; and a mandate concerned with long bear markets places more weight on persistence. In numerical work, the non-smooth indicators in (26) and (28) can be replaced by smooth logistic approximations, or handled directly by simulation-based constrained optimization.

4 Dynamic control problem

4.1 Wealth dynamics and Markov state

Let X_t denote wealth. Given directional exposure π_t and convex-overlay exposure q_t , wealth evolves as

$$\frac{dX_t}{X_{t-}} = \pi_t \frac{dS_t}{S_{t-}} + q_t \frac{dP_t}{P_{t-}}. \tag{31}$$

Using (1) and (7),

$$\begin{aligned} \frac{dX_t}{X_{t-}} &= [\pi_t \mu + q_t \mu_P(t, S_t, v_t)] dt \\ &\quad + [\pi_t + q_t \delta_P(t, S_t, v_t)] \sqrt{v_t} dW_t^S + q_t \nu_P(t, S_t, v_t) \xi \sqrt{v_t} dZ_t \\ &\quad + [\pi_t (e^\zeta - 1) + q_t R_P(t, S_{t-}, v_t; \zeta)] dN_t. \end{aligned} \quad (32)$$

The immediate post-jump wealth map is therefore

$$X_t = X_{t-} \left(1 + \pi_t (e^\zeta - 1) + q_t R_P(t, S_{t-}, v_t; \zeta) \right). \quad (33)$$

Lemma 4.1 (Strict wealth positivity under two-sided directional exposure). *Assume Assumption 2.1 and the overlay bound $R_P(t, s, v; \zeta) \geq -1$ for all admissible (t, s, v, ζ) . Then the post-jump wealth multiplier in (33) satisfies, for every admissible (π_t, q_t) and every $\zeta \in [\underline{\zeta}, \bar{\zeta}]$,*

$$1 + \pi_t (e^\zeta - 1) + q_t R_P(t, S_{t-}, v_t; \zeta) \geq \min \left\{ 1 - \bar{\pi} - \bar{q}, 1 + \underline{\pi} (e^{\bar{\zeta}} - 1) - \bar{q} \right\} > 0,$$

where the second inequality uses the leverage condition (5). Consequently, if $X_0 > 0$, the wealth process remains strictly positive almost surely on $[0, T]$.

Proof. Between jump times, X is the stochastic exponential of a continuous semimartingale and is therefore strictly positive as long as it starts positive. At a jump time, the multiplier $m(\zeta) := 1 + \pi_t (e^\zeta - 1) + q_t R_P(t, S_{t-}, v_t; \zeta)$ is the sum of three terms. The worst case for a long position ($\pi_t \geq 0$) is $\zeta = \underline{\zeta}$, which gives the bound $1 - \bar{\pi} - \bar{q}$ because $e^{\underline{\zeta}} - 1 \geq -1$ and $R_P \geq -1$. The worst case for a short position ($\pi_t < 0$) is $\zeta = \bar{\zeta}$, which gives the bound $1 + \underline{\pi} (e^{\bar{\zeta}} - 1) - \bar{q}$; this is strictly positive by (5). Both bounds depend only on fixed admissible parameters, so the multiplier is bounded away from zero uniformly in ζ and in $(\pi_t, q_t) \in \mathcal{K}$, which preserves positivity at every jump. \square

Remark 4.2 (Economic interpretation of the leverage condition). The two inequalities in (5) handle the two worst-case jump directions separately. The first, $\bar{\pi} + \bar{q} < 1$, restricts how much simultaneous long directional and overlay exposure can be admitted: in the worst-case downside jump ($e^{\underline{\zeta}} - 1 \geq -1$ combined with $R_P \geq -1$) the post-jump multiplier collapses to $1 - \bar{\pi} - \bar{q}$, which must be strictly positive. The second inequality is the symmetric constraint for a short directional position hit by the worst upside jump: it couples the lower directional bound $\underline{\pi} < 0$, the upside truncation $\bar{\zeta}$, and the overlay upper bound \bar{q} . Both inequalities are non-binding in the stylized calibration of Table 2: the annualized jump intensity and mean log-jump are negative, and the upside truncation $\bar{\zeta}$ sits several standard deviations above the mean, while the numerical experiments take $\bar{\pi} + \bar{q}$ well below 1. If the modeller wishes to permit stronger directional or overlay positions, the bounds must be reconciled through (5), e.g. by lowering \bar{q} (reducing overlay concentration) or by tightening $\bar{\pi}$ or $\underline{\pi}$. The alternative — leaving jumps unbounded and admitting wealth default — requires a different admissible class than the one used here.

The natural Markov state is now explicit:

$$U_t := (X_t, S_t, v_t, M_t) \in (0, \infty)^3 \times \mathbb{R}. \quad (34)$$

Spot must be included separately from wealth because the overlay return depends on the current asset price even when the investor is hedged. This is the main state-variable correction relative to simplified treatments that try to infer the underlying level from wealth alone.

4.2 HJB characterization

Fix the auxiliary parameter $\eta \in \mathbb{R}$ from (22). For $u = (x, s, v, m)$ define

$$V(t, u; \eta) := \inf_{(\pi, q) \in \mathcal{A}} \left\{ \eta + \frac{1}{1 - \alpha} \mathbb{E}[(-\log X_T - \eta)^+ \mid U_t = u] \right\}, \quad (35)$$

where \mathcal{A} is the admissible class induced by Assumption 2.1 and $X_0 = 1$ so that $L = -\log X_T$ as in (19). The full CVaR is recovered by the outer minimization $\text{CVaR}_\alpha(L) = \min_{\eta \in \mathbb{R}} V(t, U_t; \eta)$, so the problem has a two-level structure: the HJB below solves the inner policy optimization for each fixed η , and η is chosen in an outer step.

To write the generator compactly, define the drift vector

$$b^{\pi, q}(t, u) := \begin{pmatrix} x(\pi\mu + q\mu_P(t, s, v)) \\ \mu s \\ \kappa(\theta - v) \\ \mu - \frac{1}{2}v - \gamma m \end{pmatrix} \quad (36)$$

and the diffusion loading matrix with respect to the correlated Brownian pair (W^S, Z) ,

$$\Sigma^{\pi, q}(t, u) := \sqrt{v} \begin{pmatrix} x(\pi + q\delta_P(t, s, v)) & xqv_P(t, s, v)\xi \\ s & 0 \\ 0 & \xi \\ 1 & 0 \end{pmatrix}, \quad C := \begin{pmatrix} 1 & \rho \\ \rho & 1 \end{pmatrix}. \quad (37)$$

The local covariance matrix is $a^{\pi, q}(t, u) := \Sigma^{\pi, q}(t, u)C\Sigma^{\pi, q}(t, u)^\top$. Finally, define the jump map

$$\Gamma^{\pi, q}(t, u; \zeta) := \left(x(1 + \pi(e^\zeta - 1) + qR_P(t, s, v; \zeta)), se^\zeta, v, m + \zeta \right). \quad (38)$$

Proposition 4.3 (HJB equation in viscosity form). *Assume Assumptions 2.1 and 2.2. Suppose the coefficients of the state process satisfy the usual local Lipschitz and linear-growth conditions and that V in (35) is finite and continuous. Then V is a viscosity solution of*

$$\partial_t V + \inf_{(\pi, q) \in \mathcal{K}} \left\{ b^{\pi, q}(t, u) \cdot \nabla_u V + \frac{1}{2} \text{tr}(a^{\pi, q}(t, u) D_u^2 V) + \lambda \mathbb{E}_\zeta [V(t, \Gamma^{\pi, q}(t, u; \zeta); \eta) - V(t, u; \eta)] \right\} = 0, \quad (39)$$

with terminal condition

$$V(T, u; \eta) = \eta + \frac{1}{1 - \alpha} (-\log x - \eta)^+. \quad (40)$$

Under a comparison principle for the associated integro-PDE, this viscosity solution is unique.

Proof sketch. Under the stated regularity conditions, U_t is a controlled Markov jump diffusion. The dynamic-programming principle for controlled Markov processes then yields (39) with the generator built from the drift, diffusion covariance, and jump map above; see Fleming and Soner (2006), Pham (2009), and Øksendal and Sulem (2005). The terminal cost is kinked because of the positive-part function in (22), so viscosity rather than classical solutions are the natural solution concept. A comparison principle for the resulting integro-PDE is a standard additional assumption rather than a consequence of bounded jumps alone. Under compact controls, continuous coefficients with the growth bounds stated above, finite-activity bounded jumps, and an admissible polynomial-growth class for the value function, the required comparison result follows from the nonlocal maximum principle for semicontinuous functions of Jakobsen and Karlsen (2006) and the Jensen–Ishii lemma for integro-differential equations of Barles and Imbert (2008). Bounded jump support is used here to control the nonlocal term and finite moments of the jump measure; the remaining continuity and growth hypotheses are part of the standard viscosity-solution comparison framework for controlled jump diffusions. \square

Remark 4.4 (Why this accounting matters). The option overlay affects the HJB through *all* three channels: drift (carry), diffusion exposure, and jump repricing. This is exactly what a serious tail-risk-management model must capture. A terminal-payoff expression of the form $X_T = S_T + \theta(K - S_T)^+$ is useful for intuition, but it is not a self-financing wealth equation and cannot by itself support dynamic optimization.

Remark 4.5 (Where the four diagnostics sit in the HJB). The HJB still optimizes a single CVaR objective. The diagnostic quantities in Section 3.1 are not additional state variables unless the modeller chooses to impose them dynamically. They are lower-dimensional summaries of the same simulated or controlled return distribution: jump repricing maps into conditional convexity and hit ratio, the drift term maps into carry, and the signal dynamics map into persistence. This is why the diagnostic layer improves interpretability without changing the core state equation.

Proposition 4.6 (Classical verification for smooth candidates). *Let $E := (0, \infty)^3 \times \mathbb{R}$. For any smooth test function ϕ , define the controlled integro-differential operator*

$$\begin{aligned} (\mathcal{L}^{\pi, q} \phi)(t, u) &:= b_{\pi, q}(t, u) \cdot \nabla_u \phi(t, u) + \frac{1}{2} \operatorname{tr}(a_{\pi, q}(t, u) D_u^2 \phi(t, u)) \\ &\quad + \lambda \mathbb{E}_\zeta [\phi(t, \Gamma_{\pi, q}(t, u; \zeta)) - \phi(t, u)]. \end{aligned}$$

Fix $\eta \in \mathbb{R}$. Suppose there exists

$$W(\cdot, \cdot; \eta) \in C^{1,2}([0, T] \times E) \cap C([0, T] \times E)$$

with polynomial growth such that

$$\partial_t W(t, u; \eta) + \inf_{(\pi, q) \in \mathcal{K}} (\mathcal{L}^{\pi, q} W)(t, u; \eta) = 0$$

for $(t, u) \in [0, T) \times E$, together with terminal condition

$$W(T, u; \eta) = \eta + \frac{1}{1 - \alpha} (-\log x - \eta)_+, \quad u = (x, s, v, m).$$

Assume also that the infimum is attained by a measurable selector

$$(\pi^*, q^*) = (\pi^*, q^*)(t, u),$$

that the associated controlled state process is well posed, and that the stopped local martingales generated by Itô's formula are uniformly integrable. Then

$$W(t, u; \eta) = V(t, u; \eta),$$

and the feedback control

$$(\pi_t^*, q_t^*) = (\pi^*, q^*)(t, U_t)$$

is optimal for the inner problem.

Proof. Fix any admissible control (π, q) . Apply Itô's formula for jump diffusions to $W(t, U_t; \eta)$, stopped at a localizing sequence. Since

$$\partial_t W + \mathcal{L}^{\pi, q} W \geq 0$$

by the HJB inequality, taking expectations yields

$$W(t, u; \eta) \leq \eta + \frac{1}{1 - \alpha} \mathbb{E}[(-\log X_T - \eta)_+ | U_t = u].$$

Taking the infimum over admissible controls gives $W \leq V$.

For the feedback selector (π^*, q^*) , the HJB holds with equality. The finite-variation term in Itô's formula is then zero, and uniform integrability of the stopped martingales gives

$$W(t, u; \eta) = \eta + \frac{1}{1 - \alpha} \mathbb{E}^{\pi^*, q^*}[(-\log X_T - \eta)_+ | U_t = u].$$

Since V is the infimum over all admissible controls, the right-hand side is at least $V(t, u; \eta)$. Combined with $W \leq V$ from the previous paragraph, this yields $W = V$, and the feedback control is optimal. \square

5 Comparative statics and hybrid demand

5.1 Why puts win on impact

Proposition 5.1 (Instantaneous crash protection). *Fix a pre-jump state $u_- = (x, s, v, m)$ and controls (π, q) . If a negative log-jump $\zeta < 0$ arrives immediately, post-jump wealth is given by (33), and its directional derivative with respect to convex exposure is*

$$\frac{\partial X_+}{\partial q} = x R_P(t, s, v; \zeta). \quad (41)$$

Whenever the overlay reprices upward in the crash state, $R_P(t, s, v; \zeta) > 0$, increasing q raises post-jump wealth and lowers the corresponding one-step loss. The effect strengthens as the crash deepens if the overlay is sufficiently convex in s .

Proof. Differentiate (33) with respect to q . The sign claim is immediate. For convex overlays such as puts, deeper negative jumps raise the mark-to-market revaluation term R_P once the contract moves toward or into the money. \square

The derivative is trivial, but it sets up the key comparison with the trend channel.

Corollary 5.2 (Trend reversal threshold). *Under the odd increasing map $\pi_t = f(M_t)$, there is a whole region of crash sizes in which the trend channel remains long on impact while the put already helps. Specifically, if $M_{t-} > 0$ and*

$$-M_{t-} < \zeta < 0, \quad (42)$$

then the post-jump trend position remains positive, whereas the convex overlay still has the potential to reprice upward through $R_P(t, s, v; \zeta)$.

The economics are immediate. Puts respond state by state. Trend responds through a signal, and the signal must first move through zero. That is why trend can be late in violent reversals even when it is effective in drawn-out crises.

Remark 5.3 (Impact versus regime). Proposition 5.1 compares the two channels *at one isolated jump arrival*, conditional on the pre-jump state. That is a genuinely different object from a one-year *regime* characterized by repeated jumps, such as the flash-crash calibration used in the numerical experiments of Section 7. A regime with intensity λ experiences an expected λT jumps over the horizon; between jumps the trend signal evolves continuously, and under Lemma 2.5 it drifts toward negative values after any sustained period of negative returns. Over such a regime, trend can therefore be already defensive by the time later jumps arrive, even though on the very first jump Proposition 5.1 implies that convex insurance is the instantaneous dominant channel. Thus the “puts win on impact” statement and the numerical finding that trend does a large share of the CVaR reduction in a year-long flash-crash regime are not in tension: they describe two different conditional objects. The interior hybrid optima documented in Section 7 arise because both mechanisms contribute: trend handles the between-jump drift, convex insurance handles the impact revaluation, and the CVaR-minimizing combination balances the two.

5.2 Why trend wins in persistent drawdowns

Lemma 2.5 gives the complementary result. Under a gradual deterministic selloff, the signal follows (17) and crosses zero after the finite delay in (18). The trend overlay therefore needs time, but once the drawdown horizon exceeds $t^* - \tau$, the same signal mechanism that hurts it in jump states becomes an advantage: exposure turns progressively defensive without requiring fresh premium outlays. That is the precise sense in which trend is a hedge against *persistent* rather than *instantaneous* tail events. Remark 5.3 extends this observation to crash-prone regimes: a regime of repeated jumps still admits trend protection provided the jumps are not so closely packed that the signal has no time to react between them.

5.3 Sufficient conditions for an interior hybrid optimum

From free control to trend-following structure. Proposition 4.3 characterizes the CVaR-optimal policy when the directional control π_t is free within the compact set \mathcal{K} . Under that formulation the model is more general than a trend-following model: any progressively measurable, compactly bounded directional policy is admissible, and the trend signal M_t enters only as a state variable that the optimizer may or may not use. To represent a trend-following overlay specifically, the directional control must be restricted to depend on the signal in a monotonic way — that is, to take the form $\pi_t = g_\theta(t, X_t, S_t, v_t, M_t)$ with g_θ increasing in M_t . The simplest nontrivial instance is $\pi_t = f(M_t)$ with f odd and strictly increasing, as introduced in (13). The comparative statics of Section 5 and the simulations of Section 7 are stated for this restricted class, not for the unrestricted HJB problem. The framework thus nests two objects: the unrestricted CVaR-optimal control, which establishes a reference ceiling, and the trend-following subclass, which is the structurally interpretable policy actually implemented in practice. The reduced two-parameter family below is the further simplification used throughout the numerical work.

The full HJB problem is high dimensional. To isolate the economic content of the hybrid demand result, it is useful to consider a reduced two-parameter policy class:

$$\pi_t = af(M_t), \quad q_t = b, \quad (a, b) \in [0, \bar{a}] \times [0, \bar{b}]. \quad (43)$$

Let $L^{a,b}$ be the resulting terminal loss and define

$$J(a, b) := \text{CVaR}_\alpha(L^{a,b}). \quad (44)$$

This reduced problem is exactly the object visualized in our experimental grid search over the hybrid put weight.

Proposition 5.4 (Sufficient conditions for an interior hybrid optimum in the reduced class). *Suppose J is continuously differentiable and strictly convex on the rectangle $[0, \bar{a}] \times [0, \bar{b}]$. Assume moreover that for every fixed $b \in [0, \bar{b}]$,*

$$\partial_a J(0, b) < 0 < \partial_a J(\bar{a}, b), \quad (45)$$

and for every fixed $a \in [0, \bar{a}]$,

$$\partial_b J(a, 0) < 0 < \partial_b J(a, \bar{b}). \quad (46)$$

Then J admits a unique minimizer (a^*, b^*) satisfying $0 < a^* < \bar{a}$ and $0 < b^* < \bar{b}$.

Proof. Because J is continuous on the compact rectangle $[0, \bar{a}] \times [0, \bar{b}]$, a minimizer exists by the extreme-value theorem. Strict convexity implies that J has at most one minimizer. The boundary sign conditions (45)–(46) rule out every boundary point: the objective is decreasing when one enters the rectangle from the left or bottom edge and increasing before reaching the right or top edge. Hence the unique minimizer cannot lie on the boundary and must be interior. \square

Remark 5.5 (Status of the result). Proposition 5.4 is a formalization of the intuition that a well-behaved CVaR objective with non-trivial boundary slopes admits an interior hybrid solution; it is not a general theorem that hybrid configurations dominate pure put or pure trend allocations. Both the strict-convexity hypothesis and the two boundary-slope conditions are substantive and do not hold automatically: the first requires the CVaR objective to be strictly convex in (a, b) , which generally fails for CVaR on nonlinear-in-weight losses; the second asks that both sleeves strictly improve the tail at zero allocation and that neither dominates at maximal allocation. The proposition should therefore be read as giving *sufficient* conditions under which the numerically observed interior optima of Figure 4 are consistent with a well-posed optimization problem, rather than as a claim that interior hybrids are generically optimal.

Remark 5.6 (Economic interpretation). The two sign conditions have clear content. The first says that allowing a trend-sensitive directional overlay strictly improves tail risk relative to zero trend exposure. The second says that adding some convex insurance strictly improves tail risk relative to no insurance. When both statements are true and the reduced objective is well behaved, the optimum is genuinely hybrid rather than a corner solution.

Remark 5.7 (On the strict-convexity assumption). CVaR is convex in portfolio weights when the loss is linear in the weights, but $J(a, b)$ here involves a nonlinear dependence through the trend signal and the option repricing. Strict convexity therefore does not hold automatically; it is a regularity condition on the particular parameter combination and jump-size distribution. In the simulation section, the grid-search CVaR curves in figure 4 are visually convex and admit clear interior minima, which is consistent with the assumption holding in the stylized calibration. More generally, strict convexity can fail if the two hedge channels are nearly redundant, in which case the optimum becomes a flat ridge rather than a unique point.

Proposition 5.8 (Local characterization of a hybrid optimum in the reduced class).
Suppose

$$J(a, b) = \text{CVaR}_\alpha(L_{a,b})$$

is twice continuously differentiable on an open neighborhood of $(a^, b^*) \in (0, \bar{a}) \times (0, \bar{b})$. If*

$$\nabla J(a^*, b^*) = 0$$

and the Hessian

$$H_J(a^*, b^*) = \begin{pmatrix} \partial_{aa}J(a^*, b^*) & \partial_{ab}J(a^*, b^*) \\ \partial_{ba}J(a^*, b^*) & \partial_{bb}J(a^*, b^*) \end{pmatrix}$$

is positive definite, equivalently

$$\partial_{aa}J(a^*, b^*) > 0, \quad \det H_J(a^*, b^*) > 0,$$

then (a^*, b^*) is a strict local minimizer of J . If, in addition, J is convex on $[0, \bar{a}] \times [0, \bar{b}]$, then this local minimizer is the unique global minimizer on that rectangle.

Proof. The first statement is the standard second-order sufficient condition for a strict local minimum. If J is convex on the full rectangle, any local minimizer is automatically global. Positive definiteness of the Hessian yields local uniqueness, and convexity upgrades this to uniqueness on the admissible rectangle. \square

Remark 5.9 (Why this is sharper than global strict convexity). The point of the proposition is to separate two logically distinct issues. Local stability of the hybrid solution is governed by the Hessian at the candidate optimum, whereas global uniqueness on the admissible set requires an additional convexity argument. In applications, the first question is often the economically relevant one: whether the numerically identified hybrid point is genuinely interior and locally well pinned down.

6 CVaR policy gradients

Let $L(\boldsymbol{\theta}) := -\log X_T(\boldsymbol{\theta})$ be the terminal log-loss generated by a parameterized policy $\boldsymbol{\theta} \mapsto (\pi_{\boldsymbol{\theta}}, q_{\boldsymbol{\theta}})$, under the loss convention (19).

Theorem 6.1 (CVaR policy-gradient identity). *Assume $L(\boldsymbol{\theta})$ is almost surely continuously differentiable in $\boldsymbol{\theta}$, that its gradient is dominated by an integrable envelope in a neighborhood of the parameter of interest, and that the distribution of $L(\boldsymbol{\theta})$ is continuous at the α -quantile. Then*

$$\nabla_{\boldsymbol{\theta}} \text{CVaR}_{\alpha}(L(\boldsymbol{\theta})) = \frac{1}{1-\alpha} \mathbb{E} \left[\nabla_{\boldsymbol{\theta}} L(\boldsymbol{\theta}) \mathbf{1}_{\{L(\boldsymbol{\theta}) \geq \text{VaR}_{\alpha}(L(\boldsymbol{\theta}))\}} \right]. \quad (47)$$

Proof. Start from the Rockafellar–Uryasev representation (22). Under the dominating envelope, differentiation may be interchanged with expectation. Continuity of the loss distribution at the α -quantile ensures that the positive-part term is a.s. differentiable at $\eta^* = \text{VaR}_{\alpha}(L(\boldsymbol{\theta}))$ and that the boundary term in the interchange vanishes; see Hong and Liu (2009, Thm. 3.1) for a direct proof of (47) under these assumptions. An equivalent derivation applies the envelope theorem to the outer minimization in (22) after absorbing the optimal η^* . \square

Corollary 6.2 (Tail-gradient interpretation of hybrid demand). *In the reduced class*

$$\pi_t = af(M_t), \quad q_t = b,$$

let

$$J(a, b) := \text{CVaR}_\alpha(L_{a,b}).$$

Under the regularity conditions of Theorem 6.1,

$$\partial_a J(a, b) = \frac{1}{1 - \alpha} \mathbb{E}[\partial_a L_{a,b} \mathbf{1}\{L_{a,b} \geq \text{VaR}_\alpha(L_{a,b})\}],$$

and

$$\partial_b J(a, b) = \frac{1}{1 - \alpha} \mathbb{E}[\partial_b L_{a,b} \mathbf{1}\{L_{a,b} \geq \text{VaR}_\alpha(L_{a,b})\}].$$

Hence the first-order condition for an interior hybrid optimum is equivalent to

$$\mathbb{E}[\partial_a L_{a^*,b^*} \mathbf{1}\{L_{a^*,b^*} \geq \text{VaR}_\alpha(L_{a^*,b^*})\}] = 0,$$

$$\mathbb{E}[\partial_b L_{a^*,b^*} \mathbf{1}\{L_{a^*,b^*} \geq \text{VaR}_\alpha(L_{a^*,b^*})\}] = 0.$$

In words: at the interior hybrid optimum, neither an incremental increase in trend intensity nor an incremental increase in convex insurance improves the α -tail on average.

Proof. Apply Theorem 6.1 with parameter $\boldsymbol{\theta} = (a, b)$. □

The sample analogue should be written carefully. If \hat{q}_α is the empirical α -quantile and $N_\alpha := \sum_{i=1}^N \mathbf{1}\{L^{(i)} \geq \hat{q}_\alpha\}$, then a natural Monte Carlo estimator is

$$\widehat{\nabla_{\boldsymbol{\theta}} \text{CVaR}_\alpha} = \frac{1}{N_\alpha} \sum_{i=1}^N \nabla_{\boldsymbol{\theta}} L^{(i)} \mathbf{1}\{L^{(i)} \geq \hat{q}_\alpha\}. \quad (48)$$

Because this is the tail average of the loss gradient, it is the finite-sample object that corresponds directly to the conditional-expectation definition of CVaR. Under standard regularity conditions, it is a consistent estimator of the policy gradient; see again Hong and Liu (2009). The alternative normalization $\frac{1}{(1-\alpha)N} \sum_{i=1}^N \nabla_{\boldsymbol{\theta}} L^{(i)} \mathbf{1}\{L^{(i)} \geq \hat{q}_\alpha\}$ that drops out of (22) directly is asymptotically equivalent to (48) because $N_\alpha/N \rightarrow 1 - \alpha$ a.s. under distributional continuity at the quantile; the difference is $O_p(N^{-1/2})$ in the tail-count ratio and does not affect consistency. In practice we also use common random numbers across the w -grid in Figure 5 so that the tail-gradient curve is driven by policy changes rather than by simulation noise between grid points. In constrained problems such as $w \in [0, 1]$, projected gradient descent is immediate.

7 Stylized Monte Carlo evidence

This section reports numerical experiments that generate fast, stylized evidence for the theory. The goal is not full empirical calibration. It is to check whether a computational implementation reproduces the state ranking implied by the analytical results above.

Table 2: Stylized simulation inputs used in the experiments.

Block	Quantity	Symbol	Value
Market	Expected return	μ	0.07
Market	Initial / long-run variance	v_0, θ	0.04, 0.04
Market	Mean reversion	κ	3.0
Market	Vol-of-vol	ξ	0.40
Market	Leverage correlation	ρ	-0.70
Jumps	Intensity	λ	3.0 per year
Jumps	Mean log-jump	μ_ζ	-0.05
Jumps	Log-jump volatility	σ_ζ	0.07
Trend	Signal half-lives	—	1m / 3m / 12m
Put overlay	Moneyness / roll frequency	K/S_0	0.90, monthly
Simulation	Horizon / step / paths	—	1 year / 252 days / 2,000

These are illustrative inputs used in the experiments. They are chosen to produce realistic-looking non-Gaussian equity dynamics, not to estimate a live option surface or historical carry premia exactly. The companion replication script exposes the number of paths as a parameter; higher path counts should be used for any production statement about $\text{CVaR}_{0.99}$.

7.1 Design

The experiments simulate one-year paths at daily frequency under the model in Section 2 using 2,000 Monte Carlo paths in the baseline and three stress scenarios. For speed, the put overlay is approximated by a monthly rolled 10% OTM Black–Scholes put whose volatility input is a rolling realized-volatility proxy. Trend is implemented as an equal-weight combination of 1-, 3-, and 12-month EWMA signals on simulated log-returns. The hybrid overlay is a convex combination of the put and trend sleeves. Because the reduced policy class (43) uses a constant hybrid weight w along each path, the pre-commitment issue of Remark 3.1 is less severe in this section than in a fully reoptimized dynamic policy problem. It does not disappear conceptually: the simulated objective remains terminal CVaR , and the weight is chosen ex ante. The numerical exercise should therefore be interpreted as a pre-commitment allocation experiment over a transparent two-sleeve strategy class.

The grid search includes the pure sleeves as endpoints, so an optimized hybrid can mechanically improve on the endpoints in-sample when the CVaR curve is convex. For that reason the evidence below reports both the fixed equal-weight Hybrid in Table 3 and the optimized grid weights in Table 5. All grid points use common random numbers, which reduces Monte Carlo noise in cross-weight comparisons. In a production empirical study, the optimized weight should additionally be selected on a training period or simulation batch and evaluated on an independent holdout batch.

The baseline parameters satisfy the Feller condition $2\kappa\theta = 0.24 > 0.16 = \xi^2$ in continuous time, so the true variance process remains strictly positive almost surely. The Feller condition does not, however, carry over automatically to the discrete scheme: a plain Euler–Maruyama step on the CIR diffusion can still produce negative variance draws. We therefore discretize the variance equation using the full-truncation Euler scheme of Lord et al. (2010), which replaces $\sqrt{v_t}$ in both the diffusion and drift terms

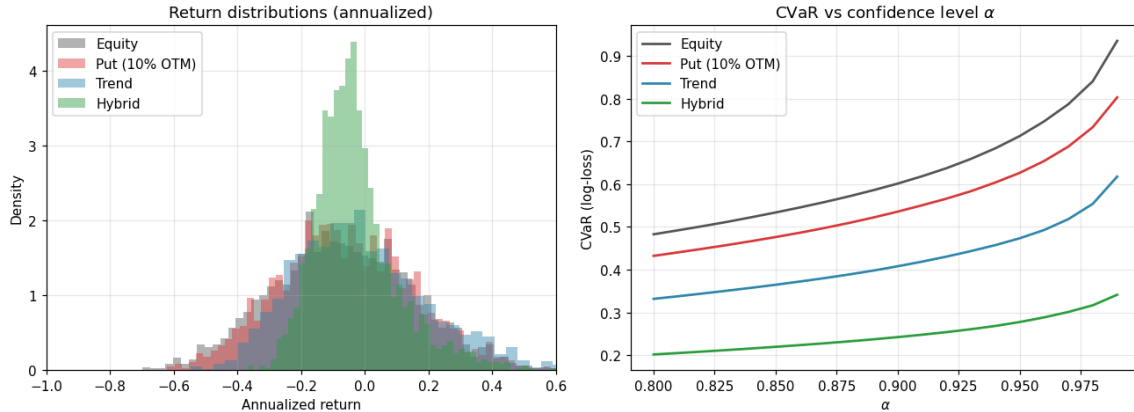


Figure 2: Baseline strategy comparison from the experiments. Left: annualized return distributions for unhedged equity, the put overlay, trend, and the hybrid. Right: CVaR as a function of the confidence level α . In the baseline, the hybrid has the lowest CVaR curve across the displayed tail levels.

Table 3: Baseline simulation outcomes from the experiments. The last column gives the nonparametric bootstrap standard error of the $\text{CVaR}_{0.95}$ estimator.

Strategy	Mean	Std	Sharpe	Skew	Kurt	VaR95	CVaR95	SE
Equity	-0.0673	0.2240	-0.300	0.165	-0.002	0.5540	0.7126	0.0211
Put (10% OTM)	-0.0569	0.2124	-0.268	0.238	0.027	0.4995	0.6265	0.0165
Trend	0.0048	0.2456	0.020	1.325	3.921	0.3861	0.4734	0.0127
Hybrid	-0.0289	0.1330	-0.217	1.216	2.663	0.2276	0.2773	0.0068

All numbers are annualized one-year path statistics from the experiments. The CVaR column uses the log-loss convention $L = -\log(X_T/X_0)$. The Hybrid allocation is an equal mix ($w = 0.5$) of the Put and Trend sleeves at the per-step return level. Bootstrap standard errors use $B = 500$ resamples. Because the design is stylized, level differences should be read qualitatively rather than as calibrated historical performance estimates.

with $\sqrt{v_t^+}$ at each step; this preserves non-negativity of the simulated variance path and has well-documented weak convergence properties for CIR-type dynamics. Alternative schemes with the same positivity property — notably Andersen’s quadratic-exponential scheme — give very similar results in the stylized calibration used here.

The baseline message is exactly the one suggested by Proposition 5.4. The hybrid strategy has the lowest baseline CVaR (0.2773), meaningfully improving on both the pure put (0.6265) and pure trend (0.4734) overlays. Trend is the best of the four on mean return in this stylized sample, while both put and hybrid overlays improve left-tail metrics substantially.

Monte Carlo uncertainty and robustness. Because the baseline differences are intentionally stylized and economically modest, it is useful to report sampling uncertainty alongside point estimates. For any strategy k , let $\widehat{C}_{k,\alpha}$ denote the simulated CVaR_α . Using B nonparametric bootstrap resamples of the simulated paths, define

$$\widehat{\text{se}}(\widehat{C}_{k,\alpha}) := \left(\frac{1}{B-1} \sum_{b=1}^B (\widehat{C}_{k,\alpha}^{(b)} - \bar{C}_{k,\alpha})^2 \right)^{1/2}, \quad \bar{C}_{k,\alpha} := \frac{1}{B} \sum_{b=1}^B \widehat{C}_{k,\alpha}^{(b)}.$$

Table 4: Four-axis hedge-quality diagnostics for the baseline experiment.

Strategy	Conv _{<i>i,α</i>}	Hit _{<i>i,α</i>}	Carry _{<i>i,α</i>}	Pers _{<i>i,h,d</i>}
Equity	0.0002	0.0000	0.0035	0.5124
Put (10% OTM)	0.3104	0.0000 [†]	0.0030	0.4764
Trend	−0.1454	0.6978	−0.0016	0.4486
Hybrid	0.0691	0.5180	0.0007	0.3039

Scores are computed on weekly returns (non-overlapping 5-day windows) aggregated from the baseline 2,000-path simulation. Conv, Hit, and Carry use $\alpha = 0.95$; Pers uses $h = 4$ weeks and $d = 0.05$. Under the convention $\text{Carry}_{i,\alpha} := -\mathbb{E}[R_i \mid (\mathcal{A}_\alpha^0)^c]$ of (27), a *positive* Carry value indicates drag outside stress, while a *negative* value indicates a positive carry premium.

[†] Scale artifact of the single-week Hit on a monthly OTM option; see discussion below (“The zero hit ratio for Equity and Put”). The convexity channel is captured instead by $\text{Conv}_{i,\alpha} = 0.31$.

Likewise, for a pair of strategies k, ℓ , it is informative to examine the bootstrap distribution of the difference

$$\widehat{\Delta}_{k,\ell,\alpha} := \widehat{C}_{k,\alpha} - \widehat{C}_{\ell,\alpha}.$$

This does not change the economic message of the section. It simply clarifies which conclusions are structural and which are numerically close. With 2,000 paths, the 0.95 tail contains about 100 observations and the 0.99 tail contains about 20 observations, so the deepest-tail curves in the figures should be read as qualitative diagnostics rather than precise estimates. In the present design, the main object of interest is the regime ordering—put impact protection, hybrid/trend strength in persistent bears, and mixed solutions in intermediate regimes—rather than the exact magnitude of small baseline CVaR gaps.

7.2 Four-axis hedge-quality diagnostics

The diagnostic framework of Section 3.1 is an interpretability layer around the scalar CVaR objective. It is useful to verify that the four dimensions—conditional convexity, tail reliability, non-stress carry, and drawdown persistence—separate the strategies in the economically expected way. Table 4 reports the four scores computed on weekly returns aggregated from the same Monte Carlo paths used for Table 3. The baseline equity return stream plays the role of the market R_M in (24)–(28). We use $\alpha = 0.95$ for the Conv/Hit/Carry diagnostics and a persistence window of $h = 4$ weeks with depth threshold $d = 5\%$.

The pattern is the expected one. The pure put sleeve has by far the highest conditional convexity (0.31), consistent with its jump-repricing mechanism $R_P(t, s, v; \zeta)$. The trend sleeve has the highest tail reliability (0.70): because trend goes short following a sustained drop, it is frequently positive in market-tail weeks even though its conditional beta is not negative. Equity has essentially zero conditional convexity by construction ($\text{Conv}_{i,\alpha} \approx 0$), since its downside and normal-state betas to itself are both equal to one. The Hybrid strategy sits between the two hedge corners on conditional convexity, reliability, and carry,

Table 5: Scenario-specific CVaR_{0.95} and optimal put weights from the experimental grid search.

Scenario	Equity	Put	Trend	Hybrid	$w_{0.90}^*$	$w_{0.95}^*$	$w_{0.99}^*$
Flash Crash	1.4411	1.1389	0.4360	0.3137	0.45	0.50	0.55
Prolonged Bear	1.1335	0.9511	0.5013	0.2854	0.55	0.55	0.60
Vol Spike	0.8756	0.7360	0.6330	0.3393	0.60	0.60	0.65

w_α^* is the grid-search optimum in the reduced hybrid class, where $w = 1$ corresponds to a pure put sleeve and $w = 0$ to a pure trend sleeve. The grid search uses $w \in \{0.00, 0.05, \dots, 1.00\}$ (spacing $\Delta w = 0.05$, 21 points) on the same 2,000-path simulation per scenario, with common random numbers across grid points. CVaR values are on the log-loss scale $L = -\log(X_T/X_0)$.

but its persistence score (0.30) sits *below* both parent sleeves and Equity rather than between them. This is consistent with the two-channel mechanism story: the put sleeve’s drawdown-window payoff is concentrated in the early part of a decline (once the contract moves into the money), while the trend sleeve’s defensive positioning builds later, after the signal has had time to cross through zero. A convex combination of the two therefore produces neither a large early revaluation nor a strongly defensive late position, so the fraction of drawdown windows with positive cumulative return declines relative to either parent taken alone. Importantly, this does not conflict with the CVaR ranking: *Pers* measures the probability of cumulative improvement *along* a drawdown window, whereas CVaR measures expected terminal loss in the tail. The Hybrid optimizes the latter and is evaluated on the former; the resulting profile is exactly what the mechanism-allocation interpretation of hybrid demand predicts — the optimum is not the best on any single axis, it is the best weighted combination under the CVaR objective.

The zero hit ratio for Equity and Put. The single-week reliability score $\text{Hit}_{i,\alpha}$ attains 0 for the Equity sleeve (as expected: being strictly equal to the market, its return is negative whenever the market is in its own lower tail) and also for the 10% OTM Put sleeve. The latter is initially surprising, but reflects the timing of option revaluation: at the moment the market enters its lower-tail week, a 10% OTM one-month put is typically still out-of-the-money in Black–Scholes terms; the payoff builds only as S moves further below the strike, as implied vol expands, or through the subsequent week’s repricing. Within a single 5-day window, net-of-premium-decay sleeve returns therefore remain non-positive almost everywhere in the lower-tail bucket. This is a known scale artifact of one-period hit ratios for OTM option overlays rather than a statement that the put sleeve does not help in stress; the convexity channel is captured instead by $\text{Conv}_{i,\alpha}$. A more robust reliability diagnostic is the event-horizon variant $\text{Hit}_{i,\alpha}^{h_{\text{ev}}} := \mathbb{P}(\prod_{k=1}^{h_{\text{ev}}} (1 + R_{i,t+k}) > 1 \mid \mathcal{A}_\alpha^0)$ with h_{ev} equal to the roll horizon of the sleeve; computing the event-horizon variant and cross-validating the ranking is left to a follow-up refinement of the accompanying experiments.

The experiments then consider three regimes designed to isolate the economics of the two hedge channels: a flash-crash regime with frequent deep negative jumps, a prolonged-bear regime with strongly negative drift and elevated variance, and a volatility-spike regime with high initial variance. The results are shown in figure 3 and table 5.

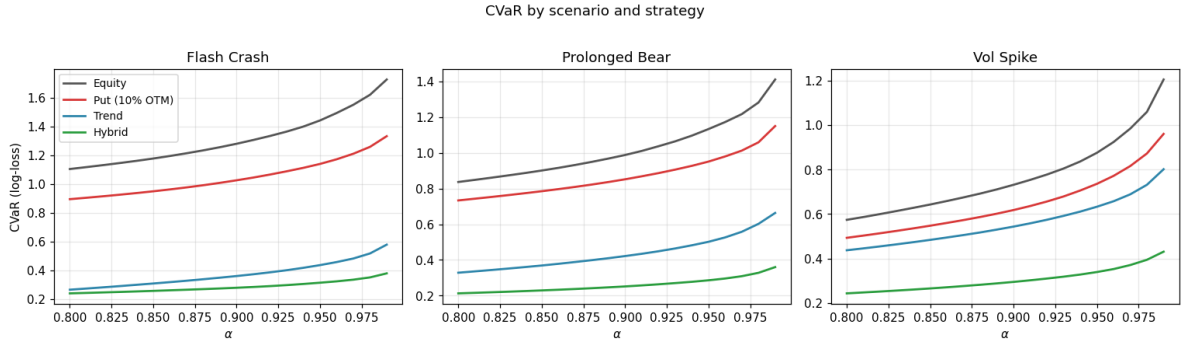


Figure 3: Scenario-specific CVaR curves in the stylized experiment. In each reported regime, the Hybrid curve lies below both pure-sleeve endpoints across the displayed α levels, consistent with the mechanism logic of Proposition 5.4. Trend alone provides substantial left-tail reduction in all three regimes; the incremental role of convex insurance is largest in the volatility-spike regime.

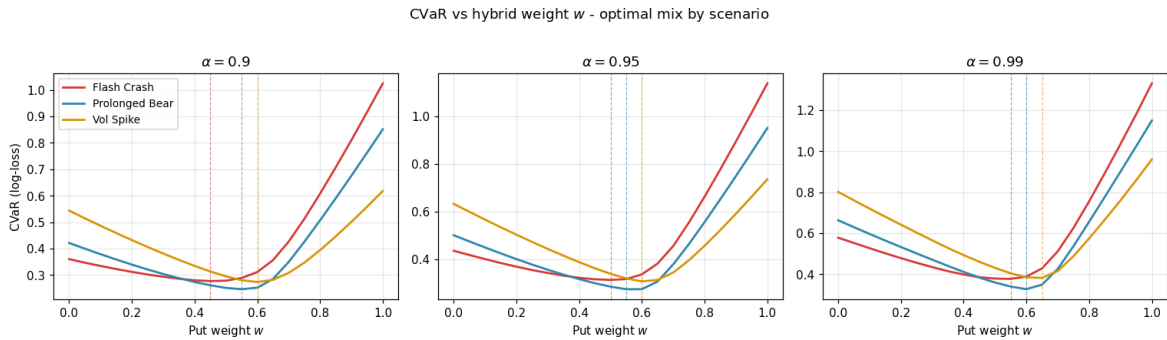


Figure 4: CVaR as a function of the put weight w in the reduced hybrid class, one panel per confidence level $\alpha \in \{0.90, 0.95, 0.99\}$. Dashed vertical lines mark the grid-search optimum w_α^* for each scenario. All curves are visibly convex in w and admit clearly interior minimizers, consistent with the assumptions of Proposition 5.4.

Three features stand out. First, in all three regimes the optimized Hybrid strategy achieves the lowest CVaR within the displayed grid, with interior optima $w^* \in [0.45, 0.65]$ — consistent with the sufficient-condition logic of Proposition 5.4, in the sense that the numerical objective exhibits the interior-minimum behavior the proposition characterizes. This is an in-simulation grid result, not a theorem of universal hybrid dominance. Its interpretation comes from the mechanism story: puts and trend are complementary rather than substitutable, and a combination of the two exploits both the instantaneous-jump protection of convex insurance (Proposition 5.1) and the persistent-drawdown protection of trend (Lemma 2.5). Second, the optimal put weight rises monotonically with tail aversion α in every scenario, reflecting the increasing marginal value of convex insurance as the investor cares about deeper losses. Third, the relative role of puts is largest in the volatility-spike regime, where the hybrid optimum sits near $w^* \approx 0.60\text{--}0.65$; by contrast, in the flash-crash regime the very large Trend reduction (CVaR falls from 1.44 to 0.44 versus 1.14 for the pure put) means that Trend does most of the work and convex insurance is the marginal complement rather than the dominant channel.

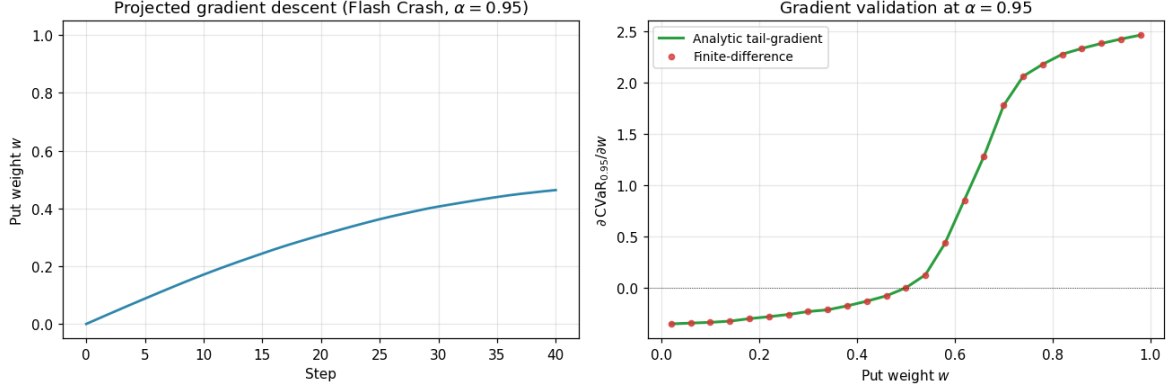


Figure 5: Policy-gradient implementation in the flash-crash regime. Left: projected gradient descent on the put weight w at $\alpha = 0.95$, starting from $w_0 = 0$ and converging monotonically to an interior optimum near $w^* \approx 0.46$. Right: the analytic tail-average CVaR gradient (Theorem 6.1) and a finite-difference benchmark overlap across the full weight grid; the sign change at w^* identifies the first-order condition numerically.

7.3 Policy-gradient implementation

The companion replication script also makes the policy-gradient result operational by optimizing the hybrid weight directly. Using the correct tail-average gradient estimator from (48), projected gradient descent in the flash-crash regime converges from the pure-trend corner $w_0 = 0$ to an interior optimum near $w^* \approx 0.46$, and the analytic tail-average gradient matches the numerical finite-difference gradient almost exactly across the full weight grid.

8 Discussion and limitations

The theoretical message of the paper is stronger than any one numerical exercise. A model that respects marked-to-market option accounting, jump risk, stochastic variance, and signal dynamics naturally produces a division of labor between puts and trend. Puts hedge states that arrive before the signal can react. Trend hedges states that last long enough for the signal to turn the portfolio defensive. The hybrid question is therefore not whether one channel is “better” in the abstract, but which channel covers which region of the tail.

At the same time, the present implementation is intentionally modest. The simulation is single-asset, not the multi-asset managed-futures environment in which trend historically shines most clearly. The current option pricer is a fast Black–Scholes proxy rather than a full Heston–jump calibration. The jump process also leaves variance itself continuous; allowing co-jumps in price and variance would be a natural extension. None of those limitations undermines the main mechanism result, but they do matter for production use.

The practical implication is that a live allocation would require an additional validation layer: option-surface calibration, transaction-cost and bid–ask stress tests, independent holdout evaluation of the selected hybrid weight, and confidence intervals for all reported CVaR improvements. The framework is meant to organize that validation, not to replace

it.

A fully empirical version of the paper would extend the present framework in three directions. First, estimate the overlay drift μ_P and jump repricing term R_P from a live index option surface. Second, move from a single-asset trend signal to the diversified multi-asset construction emphasized by Hurst et al. (2017) and Ilmanen et al. (2020). Third, allow the crash intensity λ to be regime dependent or self-exciting so that convex demand can rise endogenously into stressed states; the mutually-exciting jump-process framework of Ait-Sahalia et al. (2015) for financial contagion is a natural starting point, and connects directly to empirical evidence that tail-risk premia concentrate in clustered episodes rather than independent arrivals.

8.1 Extension to a tradable hedge universe

The two-channel model should also be viewed as the smallest member of a larger strategy-vector formulation. Let $H_t = (H_t^1, \dots, H_t^n)$ denote tradable hedge sleeves, such as listed index options, put spreads, variance or volatility exposures, dispersion trades, volatility futures, cross-asset trend, rates trend, FX trend, commodity trend, or other liquid relative-value hedges. The wealth equation becomes

$$\frac{dX_t}{X_{t-}} = \pi_t \frac{dS_t}{S_{t-}} + w_t^\top \frac{dH_t}{H_{t-}}, \quad w_t \in \mathcal{W} \subset \mathbb{R}^n, \quad (49)$$

where \mathcal{W} contains budget, leverage, liquidity, and shorting constraints. Each sleeve can be assigned a characteristic vector

$$z_i = (\text{Conv}_{i,\alpha}, \text{Hit}_{i,\alpha}, \text{Carry}_{i,\alpha}, \text{Pers}_{i,h,d}). \quad (50)$$

The structuring problem is then not simply to choose instruments, but to choose a portfolio of mechanisms. For example, a volatility sleeve may have strong conditional convexity but high carry cost; a cross-asset trend sleeve may have weaker impact protection but better persistence; and a dispersion sleeve may supply a more specific volatility-risk exposure. The optimization can select weights w directly while imposing the constraints in (29) or the penalties in (30). This turns the model into a design tool: a structured hedge can be described not only by its CVaR improvement, but by the explicit mix of convexity, reliability, carry, and persistence it delivers.

The present paper does not estimate this full characteristic matrix. Doing so would require historical or surface-implied returns for each sleeve and common stress definitions across asset classes. But the mathematical extension is straightforward: replace the scalar convex exposure q_t by w_t , augment the state by any sleeve-specific signals or volatility factors needed for Markovian dynamics, and solve the same CVaR control problem on the enlarged state space.

What is structural and what is calibration-dependent. The strongest conclusions of the paper are analytical rather than numerical. The marked-to-market accounting correction, the state augmentation to (X, S, v, M) , and the separation of two protection mechanisms — immediate jump repricing for convex insurance and delayed signal-driven

derisking for trend — all arise from the model structure itself. By contrast, the exact magnitudes of the simulated CVaR gaps, the location of the hybrid optimum, and the quantitative slope of the weight-CVaR curve are calibration-dependent. This distinction is important for interpretation. The simulations should be read as computational illustrations of the structural ranking, not as a claim that the reported weight levels or tail improvements are stable empirical constants across markets, maturities, or option-surface environments.

9 Conclusion

This paper develops a continuous-time framework for tail-risk management that puts convex option insurance and dynamic trend-following inside one coherent CVaR objective. The key modeling choice is to treat the option overlay as a traded marked-to-market asset. Once that accounting is imposed, the relevant state is not just wealth but wealth, spot, variance, and the trend signal; and once that state is written down, the economic separation of the two protection mechanisms becomes sharp.

The central mechanism story is about timing rather than dominance. On an isolated jump, convex insurance reprices contractually and immediately, while trend is necessarily late because its signal must first cross through zero (Proposition 5.1 and Corollary 5.2). Over a horizon that contains repeated jumps or a sustained drawdown, however, trend has time to react: after each shock the signal drifts toward negative values and the overlay turns defensive (Lemma 2.5). A year-long flash-crash *regime* is therefore not the same object as one jump on impact: it contains many between-jump stretches in which trend can work, and the optimal hedge over that regime is not the same as the optimal hedge against a single shock.

The stylized experimental evidence reflects exactly this picture. In the reported simulations, hybrid allocations deliver the lowest CVaR within the specified strategy grid, with interior optima near $w^* \in [0.45, 0.65]$ across baseline, flash-crash, prolonged-bear, and vol-spike calibrations. Trend accounts for a large share of the CVaR reduction in regimes with repeated jumps because it has time to react between shocks, while convex insurance adds a further improvement on top of trend and becomes relatively more valuable as the tail-aversion level α rises. The diagnostic layer explains why both channels are wanted: the put sleeve loads strongly on conditional convexity, the trend sleeve loads strongly on tail reliability, and the hybrid is the allocation that balances these mechanisms against carry and persistence. That is the kind of state-contingent answer practitioners need. Tail-risk management is not a contest between convex insurance and trend. It is an allocation problem across loss mechanisms, and in a production setting those mechanisms can be represented as a vector of tradable strategies rather than a small set of stylized instruments.

A Replication and validation checklist

The accompanying package includes a Python script, `replication_tail_risk_management.py`, that implements the same stylized simulation architecture used in Section 7: Heston-

type variance with full truncation, finite-activity jumps, rolled Black–Scholes put proxies, EWMA trend signals, hybrid weights, CVaR curves, bootstrap standard errors, and a projected-gradient illustration. The script is intentionally transparent rather than optimized. Its purpose is to make the numerical pipeline auditable and to let the reader increase the path count, alter the option-pricing proxy, or introduce transaction-cost assumptions.

For a production empirical study, the following validation steps should be reported alongside any headline CVaR improvement:

1. **Common-random-number grid.** All hybrid weights should be evaluated on the same simulated shocks so that differences across weights reflect policy changes rather than Monte Carlo noise.
2. **Holdout selection.** The weight w^* should be selected on a training batch or historical window and evaluated on an independent holdout batch or later historical window.
3. **Tail uncertainty.** CVaR estimates should be accompanied by bootstrap or asymptotic standard errors. At confidence level α , an N -path simulation uses roughly $(1 - \alpha)N$ tail observations; this is especially important for $\alpha = 0.99$.
4. **Option-surface sensitivity.** The put sleeve should be stress tested across implied-volatility premia, skew assumptions, bid–ask spreads, and roll-date conventions.
5. **Mechanism diagnostics.** The four scores (Conv, Hit, Carry, Pers) should be reported together with CVaR so that a lower tail loss is not mistaken for a single economic source of protection.

These checks separate the structural claim of the paper—convex crash protection and signal-driven drawdown protection are complementary mechanisms— from the calibration-specific claim that a particular hybrid weight is optimal in a particular market environment.

References

- Acerbi, Carlo (2002). “Spectral measures of risk: A coherent representation of subjective risk aversion”. In: *Journal of Banking & Finance* 26.7, pp. 1505–1518. DOI: 10.1016/S0378-4266(02)00281-9.
- Aiř-Sahalia, Yacine, Julio Cacho-Diaz, and Roger J. A. Laeven (2015). “Modeling financial contagion using mutually exciting jump processes”. In: *Journal of Financial Economics* 117.3, pp. 585–606. DOI: 10.1016/j.jfineco.2015.03.002.
- Artzner, Philippe, Freddy Delbaen, Jean-Marc Eber, and David Heath (1999). “Coherent measures of risk”. In: *Mathematical Finance* 9.3, pp. 203–228. DOI: 10.1111/1467-9965.00068.
- Barles, Guy and Cyril Imbert (2008). “Second-order elliptic integro-differential equations: viscosity solutions’ theory revisited”. In: *Annales de l’Institut Henri Poincaré C, Analyse non linéaire* 25.3, pp. 567–585. DOI: 10.1016/j.anihpc.2007.02.007.

- Bhansali, Vineer (2014). *Tail Risk Hedging: Creating Robust Portfolios for Volatile Markets*. New York: McGraw-Hill.
- Broadie, Mark, Mikhail Chernov, and Michael Johannes (2009). “Understanding index option returns”. In: *Review of Financial Studies* 22.11, pp. 4493–4529. DOI: 10.1093/rfs/hhp032.
- Cochrane, John H. (2005). *Asset Pricing: Revised Edition*. Princeton, NJ: Princeton University Press.
- Fleming, Wendell H. and H. Mete Soner (2006). *Controlled Markov Processes and Viscosity Solutions*. 2nd ed. New York: Springer. DOI: 10.1007/0-387-31071-1.
- Heston, Steven L. (1993). “A closed-form solution for options with stochastic volatility with applications to bond and currency options”. In: *Review of Financial Studies* 6.2, pp. 327–343. DOI: 10.1093/rfs/6.2.327.
- Hong, L. Jeff and Guangwu Liu (2009). “Simulating sensitivities of conditional value at risk”. In: *Management Science* 55.2, pp. 281–293. DOI: 10.1287/mnsc.1080.0901.
- Hurst, Brian, Yao Hua Ooi, and Lasse Heje Pedersen (2013). “Demystifying Managed Futures”. In: *Journal of Investment Management* 11.3, pp. 42–58.
- (2017). “A century of evidence on trend-following investing”. In: *Journal of Portfolio Management* 44.1, pp. 15–29. DOI: 10.3905/jpm.2017.44.1.015.
- Ilmanen, Antti, Thomas Maloney, and Adrienne Ross (July 2020). *Tail risk hedging: Contrasting put and trend strategies*. White Paper. AQR Capital Management. URL: <https://www.aqr.com/Insights/Research/White-Papers/Tail-Risk-Hedging-Contrasting-Put-and-Trend-Strategies>.
- Israelov, Roni and Lars N. Nielsen (2017). “Still not cheap: Portfolio protection in calm markets”. In: *Journal of Portfolio Management* 43.5, pp. 108–120. DOI: 10.3905/jpm.2017.43.5.108.
- Jakobsen, Espen R. and Kenneth H. Karlsen (2006). “A “maximum principle for semicontinuous functions” applicable to integro-partial differential equations”. In: *Nonlinear Differential Equations and Applications NoDEA* 13.2, pp. 137–165. DOI: 10.1007/s00030-005-0031-6.
- Lettau, Martin, Matteo Maggiori, and Michael Weber (2014). “Conditional risk premia in currency markets and other asset classes”. In: *Journal of Financial Economics* 114.2, pp. 197–225. DOI: 10.1016/j.jfineco.2014.07.001.
- Lord, Roger, Remmert Koekoek, and Dick Van Dijk (2010). “A comparison of biased simulation schemes for stochastic volatility models”. In: *Quantitative Finance* 10.2, pp. 177–194. DOI: 10.1080/14697680802392496.
- Markowitz, Harry (1952). “Portfolio selection”. In: *Journal of Finance* 7.1, pp. 77–91. DOI: 10.2307/2975974.
- Merton, Robert C. (1969). “Lifetime portfolio selection under uncertainty: The continuous-time case”. In: *Review of Economics and Statistics* 51.3, pp. 247–257. DOI: 10.2307/1926560.
- (1971). “Optimum consumption and portfolio rules in a continuous-time model”. In: *Journal of Economic Theory* 3.4, pp. 373–413. DOI: 10.1016/0022-0531(71)90038-X.

- Moskowitz, Tobias J., Yao Hua Ooi, and Lasse Heje Pedersen (2012). “Time series momentum”. In: *Journal of Financial Economics* 104.2, pp. 228–250. DOI: 10.1016/j.jfineco.2011.11.003.
- Øksendal, Bernt and Agnès Sulem (2005). *Applied Stochastic Control of Jump Diffusions*. Berlin: Springer. DOI: 10.1007/b137590.
- Pham, Huyên (2009). *Continuous-Time Stochastic Control and Optimization with Financial Applications*. Berlin: Springer. DOI: 10.1007/978-3-540-89500-8.
- Rockafellar, R. Tyrrell and Stanislav Uryasev (2000). “Optimization of conditional value-at-risk”. In: *Journal of Risk* 2.3, pp. 21–41. DOI: 10.21314/JOR.2000.038.